Bull. Mater. Sci. (2021)44:144
https://doi.org/10.1007/s12034-021-02397-3

Towards a green and cost-effective synthesis of polyanionic cathodes: comparative electrochemical behaviour of $LiFePO_4$/C, $Li_2FeP_2O_7$/C and Li_2FeSiO_4/C synthesized using methylcellulose matrix

MILOŠ MILOVIĆ[1,*], DRAGANA JUGOVIĆ[1], MILICA VUJKOVIĆ[2], MAJA KUZMANOVIĆ[1], ANA MRAKOVIĆ[3] and MIODRAG MITRIĆ[3]

[1]Institute of Technical Sciences of SASA, Belgrade 11000, Serbia
[2]Faculty of Physical Chemistry, University of Belgrade, Belgrade 11000, Serbia
[3]Vinča Institute of Nuclear Sciences—National Institute of the Republic of Serbia, University of Belgrade, Belgrade 11000, Serbia
*Author for correspondence (milos.milovic@itn.sanu.ac.rs)

MS received 29 July 2020; accepted 20 December 2020

Abstract. The polyanion cathodes for Li-ion batteries, namely $LiFePO_4$, $Li_2FeP_2O_7$ and Li_2FeSiO_4, were synthesized by very short high-temperature treatment (approximately several minutes) and subsequent quenching. Methylcellulose—a polymer with thermally driven water solubility—was used as the medium in which the precursor solutions were dispersed prior to high temperature treatment. The methylcellulose pyrolytically decomposes to carbon, thus producing the polyanion material/carbon composites of $LiFePO_4$/C, $Li_2FeP_2O_7$/C and Li_2FeSiO_4/C. The obtained powders have reduced crystallinity and significant microstructural characteristics: low crystallite size and notable microstrain. They exhibit stable electrochemical performances in both aqueous and organic electrolyte. The broadening of existing peaks in cyclic voltammetry and/or the emergence of new broad peaks was attributed to the presence of the amorphous phase in the samples. In galvanostatic charge–discharge tests, the materials provided high capacities at low current densities, while the highest rate performance was demonstrated by olivine-phosphate when compared to the other two materials.

Keywords. Polyanion cathodes; $LiFePO_4$; $Li_2FeP_2O_7$; Li_2FeSiO_4; methylcellulose; quenching.

1. Introduction

Polyanion cathode materials for Li-ion batteries offer the advantage of higher safety and higher voltage values in comparison to the oxide cathodes with the same $M^{x+/(x+1)+}$ redox pair [1]. Both higher voltage and higher stability come from strong covalent bonding within the polyanion units and these inherent characteristics have promoted investigation of different polyanion compounds: phosphates (PO_4^{3-} polyanion group), pyrophosphates ($P_2O_7^{4-}$), silicates (SiO_4^{4-}) and others. Among them, the iron-based compounds appear attractive, as Fe is abundant, inexpensive and less toxic than Co, Ni or Mn. $LiFePO_4$ has gained worldwide fame, thanks to its outstanding electrochemical features [2], and become the most widely studied cathode material for Li rechargeable batteries. On the other hand, $Li_2FeP_2O_7$ and Li_2FeSiO_4 attracted interest due to the possibility of extraction/insertion of two lithium ions per formula unit, which would lead eventually to higher storage capacities [3,4].

The rigid structure of polyanion compounds provides cycle stability on the one side but deteriorates ionic diffusion on the other; also, the insertion of polyanion units between FeO_n polyhedrons impedes electron transfer among Fe centres in the lattice [5]. As a result, unlike oxide-based cathodes, polyanion cathodes suffer considerably from the low conductivity (both ionic and electronic), which significantly limits their rate performance and therefore application in high power devices. To overcome this, for some researchers, it seemed tempting to induce a structural degradation of the polyanionic framework, to produce a disordered or defective phase and to investigate the electrochemical response. Zhang *et al* [6] offered the strategy of disorder/order engineering to improve the Li-ion battery anode performances. Xiong *et al* [7] reported the enhanced cathode storage performance of $NaFePO_4$ by mechanochemically induced disorder. Similarly, the activation of β-$LiFePO_4$ was achieved by optimized disordering via ball milling route [8]. The defective phase of olivine

Electronic supplementary material: The online version of this article (https://doi.org/10.1007/s12034-021-02397-3) contains supplementary material, which is available to authorized users.

Published online: 15 May 2021

$LiFePO_4$ prepared at low temperature [9] or under oxidizing conditions [10] can result in a completely new electrochemical signature (monophasic behaviour). Density functional theory calculations suggest that tailoring native defects through a defect-controlled synthesis or post-synthetic treatment can enhance the electrical conductivity of $LiFePO_4$ [11]. The most common defect for $LiFePO_4$ is an anti-site defect, where Li and Fe ions exchange their positions. While its presence hinders the performances of $LiFePO_4$ through the obstruction of Li channel [12], high concentration of anti-sites in Li_2FeSiO_4 or $Li_2FeP_2O_7$ may provide the additional transfer between Li layers [13,14] and also reduce stress during cycling [15].

This study aimed to synthesize polyanion powders of $LiFePO_4$, $Li_2FeP_2O_7$ and Li_2FeSiO_4 with reduced crystallinity. Inspired by the previous work on the subject, we utilized a method that consists of short high-temperature treatment of the precursors dispersed in a methylcellulose matrix and subsequent quenching. The interval of high temperature treatment–which usually takes several hours to obtain the above-mentioned polyanion phases [2–4,13,14,16]—is reduced to several minutes. The usage of methylcellulose (or other cellulose ethers) is known in the literature for the structure control during ceramic processing [17,18], but seldom for the synthesis of polyanion cathodes [19]. Being water-soluble, non-toxic and inexpensive (note that cellulose is the most abundant polymer on Earth), the methylcellulose proved its worth as a carbon source in our previous investigations on electrical properties of the composites [20,21]. The method that was originally developed for Li_2FeSiO_4 [21] is now re-optimized for the group of polyanion cathode materials. The details of the chemical and technical procedures, as well as structural/microstructural examination and a comparison of their electrochemical properties, are given in the following text.

2. Experimental

The synthetic procedure consists of two basic steps: (1) precursor preparation in a methylcellulose polymer matrix and (2) short dwell at high temperature. All technical information regarding the chemicals and synthetic conditions that were used are given in table 1. In the first step, stoichiometric amounts of precursor compounds were dissolved in water and mixed with the previously prepared methylcellulose solution. The methylcellulose to inorganic precursor components mass ratio was kept the same (≈ 0.2) for all the three samples (the ratio value corresponds to the value from the sample with the highest content of carbon in [21]). The solution was stirred at ~ 70°C until gel was formed. The methylcellulose is a derivative of cellulose with the superb solubility properties in aqueous media. Unlike cellulose, the methylcellulose is a water-soluble polymer with an ability to gel upon heating and reversibly liquefy upon cooling [22], due to the hydrophobic interaction

Table 1. Summary of synthesis conditions.

Sample	Starting compounds	Pre-treatment	Thermal treatment
$LiFePO_4$/C	$FeSO_4{\cdot}7H_2O$ (Sigma-Aldrich, $\geq$ 99.0%), LiH_2PO_4 (Sigma-Aldrich, $\geq$ 99.0%) Methylcellulose (Dow, Methocel™, A4C)	Sol–gel; magnetic stirring for several hours at 60–70°C until all water evaporated	700°C, dwell time: 10min; flowing Ar + 5%H_2 (flow rate $\sim$0.1 dm^3 min^{-1})
$Li_2FeP_2O_7$/C	$FeSO_4{\cdot}7H_2O$ (Sigma-Aldrich, $\geq$ 99.0%), LiH_2PO_4 (Sigma-Aldrich, $\geq$ 99.0%) Methylcellulose (Dow, Methocel™, A4C)	As above	650°C, dwell time: 30 min; flowing Ar + 10%H_2 (flow rate $\sim$0.1 dm^3 min^{-1})
Li_2FeSiO_4/C	$Fe(NO_3)_3{\cdot}9H_2O$ (Alfa Aesar, $\geq$ 98.0%), Li_2CO_3 (Alfa Aesar, $\geq$ 99.0%), $Si(OC_2H_5)_4$–TEOS (Alfa Aesar, 99.9%), Methylcellulose (Dow, Methocel™, A4C)	As above	750°C, dwell time: 10 min, flowing Ar + 5%H_2 (flow rate $\sim$0.1 dm^3 min^{-1})

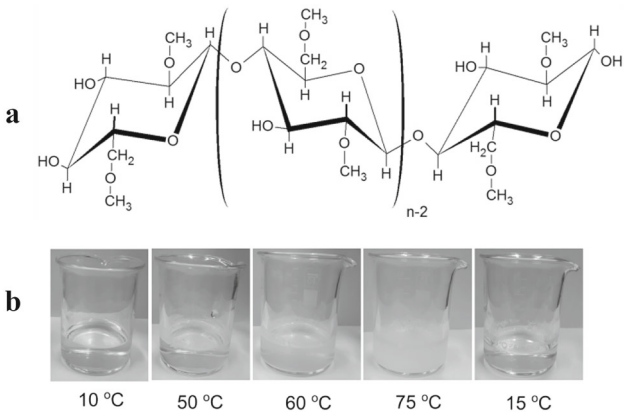

Figure 1. (**a**) Molecular structure of methylcellulose and (**b**) temperature dependence of methylcellulose' aqueous solubility.

between molecules containing methoxyl groups (figure 1). Thanks to this ability of methylcellulose, we were able to homogeneously mix the precursor compounds on a molecular level and uniformly disperse them inside a methylcellulose matrix. The methylcellulose thus serves as an excellent gelating agent, which later on, in the second step, pyrolytically degrades to carbon. The second step consists of the following: the dried gel was grounded and then introduced to a furnace at high temperature, later was kept for a short duration of time in a flowing, slightly reducing atmosphere ($Ar + H_2$) and then subsequently quenched to room temperature. Duration of the heating step for Li_2FeSiO_4 and $LiFePO_4$ samples was approximately 10 min. For $Li_2FeP_2O_7$ sample, the high-temperature dwell time had to be prolonged to 30 min due to the substantial amount of impurities that were obtained for the shorter periods of high-temperature treatment (see supplementary data for more information).

The X-ray powder diffraction measurement was performed on a Philips PW 1050 X-ray powder diffractometer using Ni-filtered Cu Kα radiation and Bragg-Brentano focusing geometry. The diffraction intensity was recorded in the 2θ range of 10°–70° with a step size of 0.02° and a counting time of 3 s per step. Powder Cell software was used for determination of the constants of the lattice. The microstructural parameters, namely the crystallite size and the microstrain, were calculated based on the fundamental parameters convolution approach to generate line profiles [23] by using the XFIT-Koalariet software. Fityk program was used for the deconvolution of X-ray diffraction (XRD) profile to crystalline and amorphous part. The carbon content was determined thermogravimetrically. The morphology of the synthesized powders was analysed by a field-emission scanning electron microscope (FESEM, TESCAN, MIRA3 XMU) at 20 kV. The particle size distributions were determined by a laser-diffraction-based particle size analyzer, Mastersizer 2000 (Malvern Instruments Ltd., UK).

The electrochemical measurements were conducted by using Vertex. One potentiostat/galvanostat with an impedance analyzer (Ivium Technologies). Cyclic voltammetry (CV) measurements were performed in a three-electrode cell with platinum as a counter and SCE (saturated calomel electrode, SI Analytics) as a reference electrode; 6 M solution of $LiNO_3$ (Alfa Aesar 99%) in H_2O was used as an electrolyte. Chronopotentiometric (CP) measurements were carried out in a closed, argon-filled two-electrode cell with metallic Li as a counter electrode and 1 M solution of $LiClO_4$ (Fluka, p.a.) in PC (propylene carbonate, Sigma-Aldrich 99.7%) as an electrolyte. Working electrode for both CP and CV measurements consisted of the active material, carbon black and poly-vinylidenefluoride (PVDF, Sigma-Aldrich) mixed in 85:10:5 weight ratio and deposited on a platinum foil from the slurry prepared in N-methyl-2-pyrrolidone (Sigma-Aldrich, 99%). Electrochemical impedance spectroscopy (EIS) was performed in the frequency range from 10^5 to 10^{-2} Hz with an amplitude of 5 mV and at open-circuit conditions of two-electrode cell with the same setup as in CP measurements.

3. Results and discussion

The presented gel-combustion procedure gives rise to similar morphologies of the obtained powders, as revealed by field emission scanning electron microscopy (figure 2). The particles are agglomerated and irregular in shape. Particle bonding and neck generation, indicating inter-particle sintering, leads to a formation of irregularly shaped pores of variable widths. The particle size distributions have a lognormal shape (figure 2d) with close span values of 1.09–1.27 (table 2). Distribution profiles of Li_2FeSiO_4/C and $LiFePO_4$/C practically overlap each other, while $Li_2FeP_2O_7$/C is a bit shifted in terms of particle size and span.

The crystal phases of the synthesized powders were confirmed by X-ray powder diffraction (figure 3). In $LiFePO_4$/C sample, $LiFePO_4$ olivine phase (orthorhombic space group no. 62, *Pnma*) was revealed along with the traces of $Fe_2P_2O_7$ and Li_3PO_4 (altogether less than 5 wt%). In Li_2FeSiO_4/C sample, Li_2FeSiO_4 phase crystallized in a monoclinic space group no. 14 ($P2_1/c$), which corresponds to the γ_s polymorph of the material [24]; besides the desired phase, traces of Li_2SiO_3 were observed (< 2 wt%). In the last sample, $Li_2FeP_2O_7$ phase crystallized within the same space group no. 14 ($P2_1/c$) and was accompanied by the olivine $LiFePO_4$ phase in the amount of 9–10 wt%. Extended heat treatment (from 10 to 30 min) of the $Li_2FeP_2O_7$/C sample brought reduction of impurities, but not a complete removal of olivine phase (supplementary data). Since both phases are capable of Li intercalation and our plan was to synthesize powders with significant microstructural parameters, further prolongation of the heat treatment was avoided. The creation of significant amount of side products during synthesis of $Li_2FeP_2O_7$/C indicate,

however, a higher complexity, and thus slower kinetics of formation of pyrophosphate $Li_2FeP_2O_7$ phase than olivine $LiFePO_4$, although starting from the same precursor compounds (table 1).

The calculated unit cell parameters (table 2) are fairly consistent with earlier reports for the given phases. The obtained unit cell volumes are however slightly lower than in annealed powders (335.65 $Å^3$ for Li_2FeSiO_4 [25], 291.44 $Å^3$ for $LiFePO_4$ [16] and 1034.00 $Å^3$ for $Li_2FeP_2O_7$ [20]), which might be related to the significant quantity of strain that is observed (table 2). There was no evidence for the formation of crystalline carbon in the samples, therefore the internal non-graphitic carbon could be assumed to contribute to the background of XRD patterns. The amounts of the *in-situ*-formed carbon, established thermogravimetrically, were found to be 13, 10 and 8 wt% for Li_2FeSiO_4/C, $LiFePO_4$/C and $Li_2FeP_2O_7$/C, respectively. The crystallinity of a given sample was quantitatively estimated by resolving the diffraction intensity profile into contributions from the crystalline (sharp) diffractions and amorphous (diffuse) halo; the degree of crystallinity then equals the ratio of area of crystalline fraction to sum of areas of crystalline and amorphous fractions. The estimated values of crystallinity with regard to carbon content of the samples suggest that lattice distortions also contribute to the amorphous halo (table 2). The $Li_2FeP_2O_7$/C sample has somewhat higher degree of crystallinity, along with larger crystallite and particle size, probably due to the longer heat exposure. Because of the different chemistries involved, the comparisons from table 2 are not straightforward, but we can make some general comments: (a) fraction of amorphous phase, small crystallite size and notable microstrain confirm that the presented method yields powders with pronounced microstructural parameters; (b) in a given range of

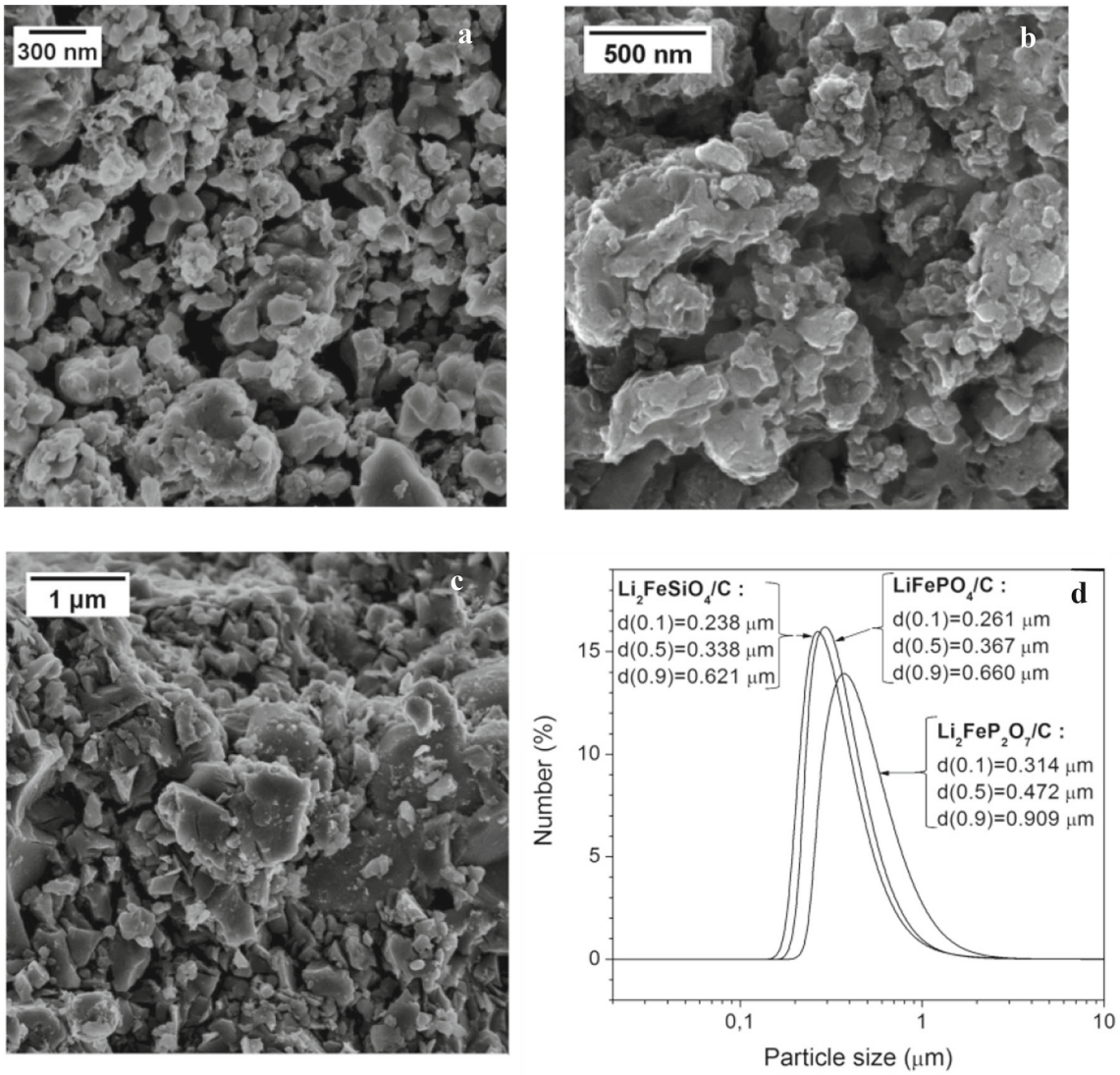

Figure 2. SEM micrographs of (**a**) Li_2FeSiO_4/C, (**b**) $LiFePO_4$/C, (**c**) $Li_2FeP_2O_7$/C and (**d**) their particle size distributions.

Table 2. Structural and microstructural parameters of the prepared powders.

Sample	Carbon content (wt%)	Lattice parameters		Crystallinity (%)	Mean crystallite size (nm)	Microstrain (%)	Mean particle size (μm)	Span*
Li_2FeSiO_4/C	13	$P2_1/c$	$a = 8.220$Å $b = 5.008$ Å $c = 10.690$ Å $\beta = 130.475°$ $V = 334.767$ Å^3	80	27	0.16	0.353	1.13
$LiFePO_4$/C	10	*Pnma*	$a = 10.325$ Å $b = 6.0053$Å $c = 4.691$ Å $V = 290.884$ Å^3	87	46	0.20	0.367	1.09
$Li_2FeP_2O_7$/C	8	$P2_1/c$	$a = 11.023$ Å $b = 9.756$ Å $c = 9.807$ Å $\beta = 101.545°$ $V = 1033.306$ Å^3	89	58	0.08	0.472	1.26

*Span = {d(0.9) − d(0.1)}/d(0.5).

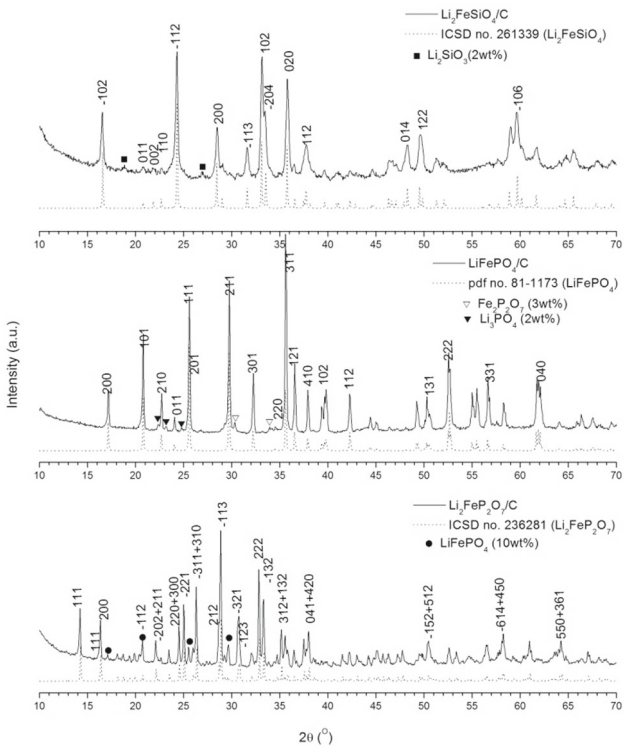

Figure 3. X-ray diffraction patterns of the obtained powders (solid line) and corresponding profiles taken from a crystallographic database (dotted line). The most prominent peaks are indexed in $P2_1/c$ (for Li_2FeSiO_4 and $Li_2FeP_2O_7$) and *Pnma* ($LiFePO_4$) symmetry group and observed impurity peaks are marked with a geometrically shaped signs.

temperatures 650–750°C, the dwell time had primary role to agglomeration and crystallite growth than temperature value itself (see $Li_2FeP_2O_7$/C, which has the largest crystallites/particles although obtained at the lowest temperature, or Li_2FeSiO_4/C and $LiFePO_4$/C, which are obtained at different temperatures but with the same dwell time and both with similar particle size distributions); (c) the increase of carbon amount leads to a decrease of crystallite and particle size.

Redox behaviour of the synthesized polyanionic composites was first evaluated by the CV measurements in an aqueous electrolyte. All materials showed the electrochemical activity caused by the Fe^{3+}/Fe^{2+} redox pair. It can be observed from figure 4 that the redox process is strongly influenced by the chemical environment in a polyanion-based compound. When a FeO_n polyhedron is coordinated with the $[SiO_4]^{4-}$ polyanions, the Fe^{3+}/Fe^{2+} redox process in Li-containing electrolyte is evidenced at −0.55/−0.32 V potentials *vs.* SCE at the scan rate of 10 mV s^{-1} (figure 4a). The amount of lithium (x) that can be reversibly removed upon this redox process may vary between $0 < x < 1$, depending on the scan rate, since the removal of lithium above 1 occurs at higher potentials. The peak potential separation of 180 mV at 2 mV s^{-1} was found to be considerably smaller than that obtained for the carbon-coated Li_2FeSiO_4 (370 mV at 0.1 m Vs^{-1} in an aqueous electrolyte) prepared via citric acid-assisted method followed by 7 h thermal treatment [26]. It indicates faster charge transfer of our sample with approximately equal (13:14) carbon content, but prepared under rapid heating regime. However, the specific capacity of Li_2FeSiO_4/C sample measured galvanostatically in an organic electrolyte (see figure 6

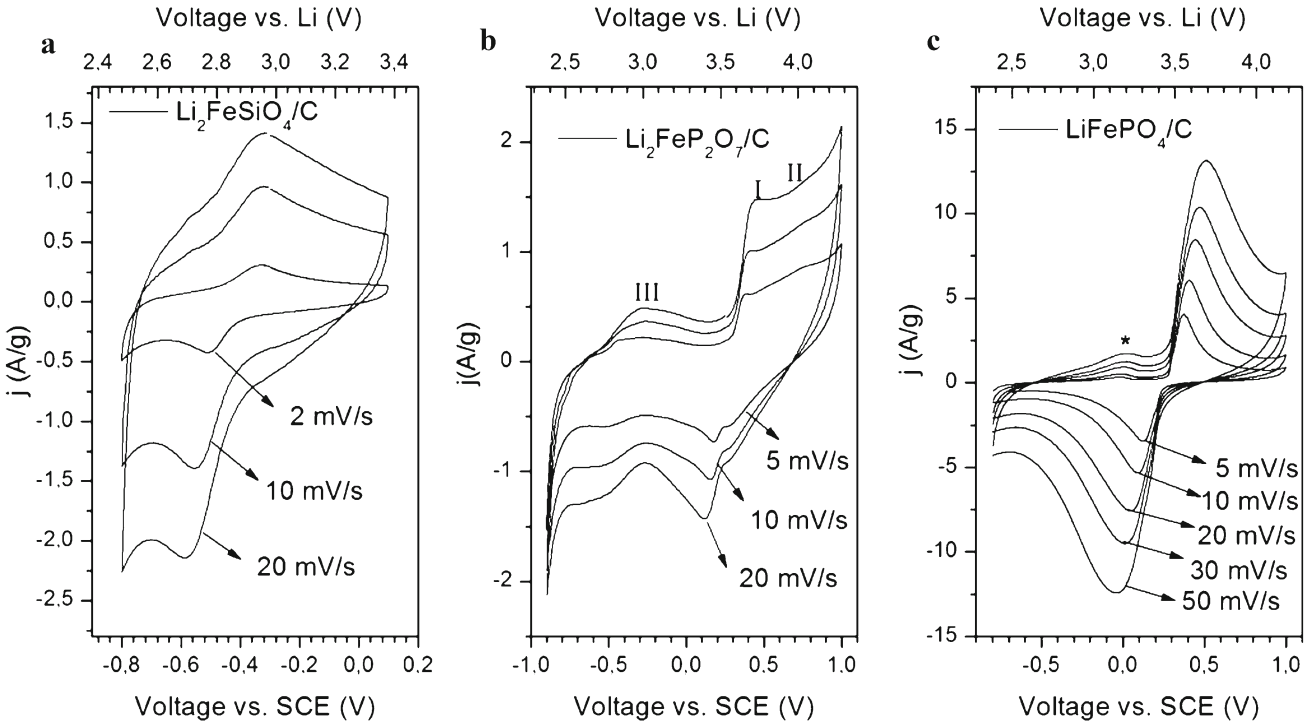

Figure 4. Cyclic voltammograms of the obtained composites at various scan rates; the potential *vs.* Li (top *x*-axis) is calculated from the measured potential *vs.* SCE (bottom *x*-axis) on the basis of reference tables of standard electrode potentials in aqueous solutions *vs.* normal hydrogen electrode [30].

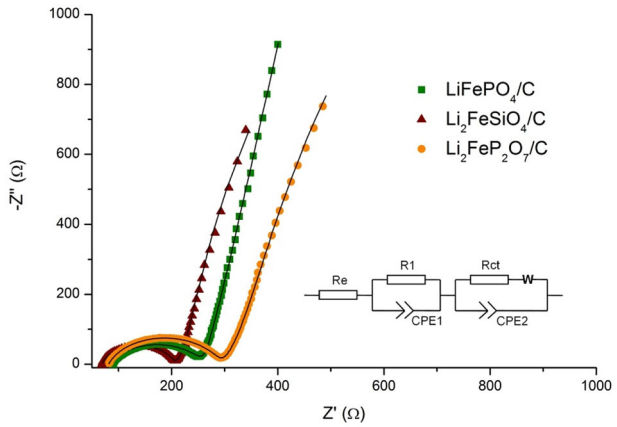

Figure 5. The Nyquist plots of the prepared two-electrode cells and the equivalent circuit scheme used in EIS analysis (inset).

below) was found to be comparable in the same voltage range to that obtained by the authors in [26], which conveys that diffusion of Li^+ in the bulk of the material is still a limiting factor for the intercalation kinetics. The peak potential separation of the other two samples is slightly higher (~240 mV in the given scan rate) than that of Li_2FeSiO_4/C, which suggest higher resistance of the charge transfer probably caused by the lower amount carbon and larger crystallites/particles.

Due to the higher electronegativity of P *vs.* Si (inductive effect), the redox potential of Fe^{3+}/Fe^{2+} is shifted towards a more positive value in phosphates than in silicates, and due to the increased electron delocalization in P_2O_7 (than in PO_4) to even more positive values in pyrophosphate compound [1]. One can see in figure 4b, the two main redox peaks (labelled as I and II) of lithium iron pyrophosphate are positioned at 0.16/0.39 and 0.28/0.69 V *vs.* SCE (10 mV s^{-1}); these characteristic peaks, partially merged together into a single broad peak, originate from Fe^{3+}/Fe^{2+} pair in FeO_6 octahedral and FeO_5 bipyramidal coordination, respectively [27]. There is, however, a third peak (III) occurring at a lower potential of −0.55/−0.26 V *vs.* SCE at 10 mV s^{-1}, which is not commonly seen in the literature data of $Li_2FeP_2O_7$ (the small peak can be seen in [28], but it is not commented). Interestingly, the occurrence of a similar peak is observed for $Na_2FeP_2O_7$ phase and is prescribed to a single-phase reaction of (de)sodiation, while the peaks at higher potentials are related to the two-phase reactions [29]; the whole profile, although somewhat shifted, much resembles our $Li_2FeP_2O_7$/C.

In figure 4c, one can notice characteristic redox peaks of $LiFePO_4$ olivine phase, which correspond to the well-known galvanostatic plateau at ~3.4 V *vs.* Li. The current response of $LiFePO_4$/C sample is significantly higher than that measured for Li_2FeSiO_4/C and $Li_2FeP_2O_7$/C samples. This indicates a significantly higher amount of stored charge in olivine compared to other two samples under a common current regime (note that a regular scan rates of several mV s^{-1} in CV correspond to high current rates in

Table 3. The fitted kinetic parameters obtained from EIS.

Sample	R_e (Ω)	R_1 (Ω)	CPE1 (s^{N1} Ω^{-1})	N1	R_{ct} (Ω)	Z_w (Ω $s^{-1/2}$)	CPE2 (s^{N2} Ω^{-1})	N2
Li_2FeSiO_4/C	69.12	1.00×10^4	8.824×10^{-3}	0.98	135.5	34.8	7.919×10^{-6}	0.85
$LiFePO_4$/C	84.27	9.27×10^4	4.596×10^{-3}	0.93	173.9	15.7	3.592×10^{-5}	0.72
$Li_2FeP_2O_7$/C	81.61	1.18×10^4	2.146×10^{-2}	0.95	208.7	30.8	2.113×10^{-5}	0.79

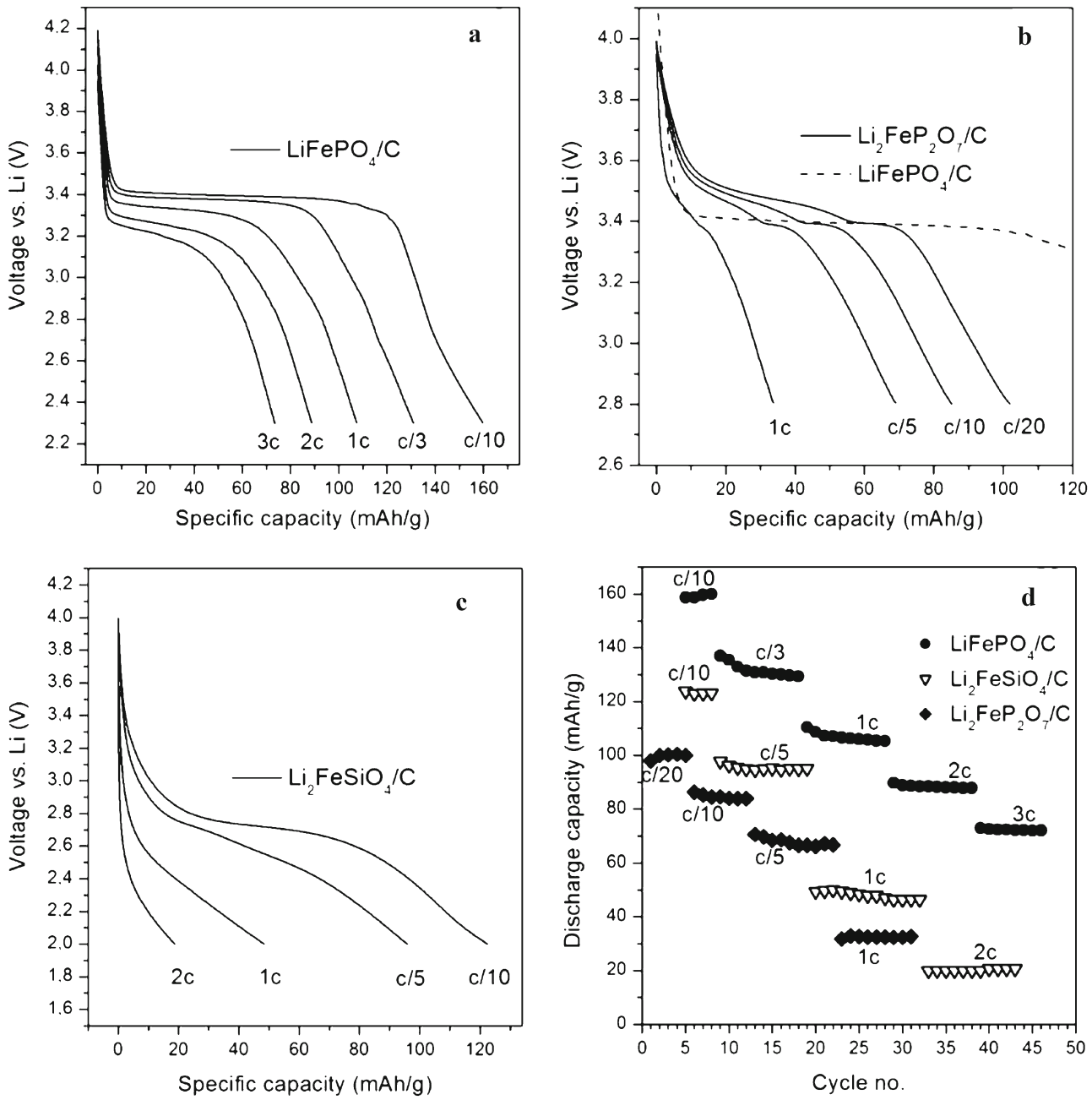

Figure 6. Discharge curves of the (**a**) $LiFePO_4$/C, (**b**) $Li_2FeP_2O_7$/C, (**c**) Li_2FeSiO_4/C and (**d**) their cycling performance.

galvanostatic cycling, > 1*c*). An additional, small and broad oxidation peak (marked with an asterisk) also appears at a potential of ≈0 V *vs.* SCE (10 mV s^{-1}), which can be attributed to the presence of the amorphous olivine phase [31]. Now, if we look back to our previous voltammogram (figure 4b) and take into consideration that amorphous olivine exhibits a single-phase reaction behaviour [10,32], by analogy we could assume that the unknown peak (III) originates from amorphous $Li_2FeP_2O_7$, which would also be consistent with the reports regarding single-phase reaction of $Na_2FeP_2O_7$ [29].

After proved electrochemically both active and stable during CV measurements in aqueous electrolyte, the materials were tested as cathodes in Li-ion cell by galvanostatic charge–discharge tests in an organic electrolyte. Prior to galvanostatic tests, the assembled cells were examined by EIS at open circuit voltages. The impedance response is shown in figure 5. Each plot is composed of a depressed semicircle in the high-to-intermediate frequency region, followed by an inclined line at the lower frequencies. The impedance data were fitted with the equivalent circuit, shown in the inset of figure 5. The equivalent circuit model includes: (1) resistor R_e, which represents the sum of electrolyte resistance and the resistance of metallic contacts; (2) resistor R_1 paralleled with the constant phase element CPE1, which is related to the cathode composite and metal (Pt) current collector interface and/or solid electrolyte interface (SEI) film phenomena [33,34]; (3) resistor R_{ct} paralleled with the constant phase element CPE2 and in serial with the general Warburg impedance Z_W, related to the cathode/electrolyte charge transfer resistance, double-layer capacitance and Li^+ solid-phase diffusion [35]. The inclusion of the constant phase elements, instead of pure capacitors, ensured a better fitting to the experimental data, as they better describe a real electrochemical system [34]. The charge transfer resistance of the tested electrode composites decreases in order $Li_2FeP_2O_7$/C > $LiFePO_4$/C > Li_2FeSiO_4/C (table 3), due to the reduction of crystallite/particle size and increase of conductive carbon concentration, both facilitating electron transfer. On the other hand, the lowest Warburg impedance for olivine composite indicates faster diffusion kinetics of this material.

The galvanostatic tests were performed at the room temperature in 4.0–2.8 V, 4.2–2.3 V and 4.0–2.0 V voltage range for $Li_2FeP_2O_7$/C, $LiFePO_4$/C and Li_2FeSiO_4/C composites, respectively. From the obtained chronopotentiometric curves at the given current rate, the specific capacities were calculated using the mass of the active material only (mass of carbon is subtracted from loading). The discharge curves along with the cycling performances are presented in figure 6. The current rates are given in *c/n* units, where *c* is a 1-electron theoretical capacity of the material (which is 166, 170 and 110 mAh g^{-1} for Li_2FeSiO_4, $LiFePO_4$ and $Li_2FeP_2O_7$, respectively) and *n* is a discharge time given in hours needed for a complete discharge. Discharge profile of $LiFePO_4$/C is distinguished by a flat plateau at around 3.4 V *vs.* Li (figure 6a), a mark of the two-phase process of lithium insertion/extraction reaction [2]. On the other side, sloping curves of Li_2FeSiO_4/C and $Li_2FeP_2O_7$/C (figure 6b and c) suggest a monophasic reaction [36,37]. Due to the presence of $LiFePO_4$ (rather than some phase transformations), the sloping curve of $Li_2FeP_2O_7$/C changes to a plateau at 3.4 V *vs.* Li (figure 6b), which makes this electrode a hybrid one. The materials were stable and performed reasonably well in accordance with its intrinsic capabilities. At low current densities, the capacities of 160 mAh g^{-1} (at *c*/10) for $LiFePO_4$/C, 124 mAh g^{-1} (*c*/10) for Li_2FeSiO_4/C and 101 mAh g^{-1} (*c*/20) for $Li_2FeP_2O_7$/C were obtained. Upon the increase of current rate, $LiFePO_4$/C powder exhibits the highest capacity preservation: 94% (at *c*/10), 80% (*c*/3), 65% (1*c*), 53% (2*c*) and 42% (3*c*). When compared to remarkable olivine, both $Li_2FeP_2O_7$/C and Li_2FeSiO_4/C show significantly lower performances (figure 6d). Although low in nominal specific capacity (due to the high molar mass of $Li_2FeP_2O_7$), the $Li_2FeP_2O_7$/C exhibits 92% utilization of its theoretical capacity at low current density. At different current rates, both $Li_2FeP_2O_7$/C and Li_2FeSiO_4/C utilize 75–77% (*c*/10), 60–63% (*c*/5) and 29–31% (1*c*) of its theoretical capacities. The capacity retention at the given rate was high for all the materials.

4. Conclusions

The polyanion cathode material's composites with carbon, namely, $LiFePO_4$/C, $Li_2FeP_2O_7$/C and Li_2FeSiO_4/C, were obtained by performing the experiments under extreme conditions of rapid heating, short high-temperature dwell and quenching to room temperature. A methylcellulose, water-soluble derivative of cellulose, was used as a polymer medium and a carbon source. The composites that were obtained have reduced crystallinity, with low crystallite size (20–60 nm) and significant microstrain (0.1–0.2). They provided stable electrochemical performance in both aqueous and organic electrolyte. The presence of amorphous phase induced spreading of existing peaks and/or the emergence of new broad peaks in CV. $LiFePO_4$/C powder exhibited superb electrode performance when compared to the $Li_2FeP_2O_7$/C and Li_2FeSiO_4/C samples. It manifests in significantly higher currents per gram provided in CV measurements and higher both capacity and capacity *vs.* current retention in galvanostatic charge–discharge tests. The potential application of Li_2FeSiO_4/C and $Li_2FeP_2O_7$/C composites thus may be limited to low power devices.

Acknowledgements

We acknowledge The Ministry of Education, Science and Technological Development of the Republic of Serbia for

providing financial support for this study, under contract no: 451-03-68/2020-14/200175 and under Bilateral Cooperation Project entitled 'Developments of novel materials for alkaline-ion batteries'.

References

[1] Gutierrez A, Benedek N A and Manthiram A 2013 *Chem. Mater.* **25** 4010
[2] Padhi A K, Nanjundaswamy K S and Goodenough J B 1997 *J. Electrochem. Soc.* **144** 1188
[3] Nishimura S, Nakamura M, Natsui R and Yamada A 2010 *J. Am. Chem. Soc.* **132** 13596
[4] Nytén A, Abouimrane A, Armand M, Gustafsson T and Thomas J O 2005 *Electrochem. Commun.* **7** 156
[5] Zaghib K, Mauger A, Goodenough J B, Gendron F and Julien C M 2007 *Chem. Mater.* **19** 3740
[6] Zhang Y, Wang P, Zheng T, Li D, Li G and Yue Y 2018 *Nano Energy* **49** 596
[7] Xiong F, An Q, Xia L, Zhao Y, Mai L, Tao H *et al* 2019 *Nano Energy* **57** 608
[8] Guo H, Song X, Zhuo Z, Hu J, Liu T, Duan Y *et al* 2016 *Nano Lett.* **16** 601
[9] Gibot P, Casas-Cabanas M, Laffont L, Levasseur S, Carlach P, Hamelet S *et al* 2008 *Nat. Mater.* **7** 741
[10] Amisse R, Sougrati M T, Stievano L, Davoisne C, Dražič G, Budič B *et al* 2015 *Chem. Mater.* **27** 4261
[11] Hoang K and Johannes M 2011 *Chem. Mater.* **23** 3003
[12] Jensen K M Ø, Christensen M, Gunnlaugsson H P, Lock N, Bøjesen E D, Proffen T *et al* 2013 *Chem. Mater.* **25** 2282
[13] Jugović D, Milović M, Ivanovski V N, Avdeev M, Dominko R, Jokić B *et al* 2014 *J. Power Sources* **265** 75
[14] Dabas P and Hariharan K 2014 *RSC Adv.* **4** 14348
[15] Ferrari S, Capsoni D, Casino S, Destro M, Gerbaldi C and Bini M 2014 *Phys. Chem. Chem. Phys.* **16** 10353
[16] Jugović D, Mitrić M, Milović M, Cvjetićanin N, Jokić B, Umićević A *et al* 2017 *Ceram. Int.* **43** 3224
[17] Cyster L A, Grant D M, Howdle S M, Rose F R A J, Irvine D J, Freeman D *et al* 2005 *Biomaterials* **26** 697
[18] Li Y, Guo Z, Hao J and Ren S 2008 *J. Mater.* **208** 457
[19] Kotobuki M, Mizuno Y, Munakata H and Kanamura K 2011 *Electrochemistry* **79** 467
[20] Jugović D, Mitrić M, Milović M, Ivanovski V N, Škapin S, Dojčinović B *et al* 2019 *J. Alloys Compd.* **786** 912
[21] Milović M, Jugović D, Mitrić M, Dominko R, Stojković-Simatović I, Jokić B *et al* 2016 *Cellulose* **23** 239
[22] Takahashi M, Shimazaki M and Yamamoto J 2001 *J. Polym. Sci. Phys.* **39** 91
[23] Cheary R W and Coelho A 1992 *J. Appl. Crystallogr.* **25** 109
[24] Islam M S, Dominko R, Masquelier C, Sirisopanaporn C, Armstrong A R and Bruce P G 2011 *J. Mater. Chem.* **21** 9811
[25] Milović M D, Vasić Anićijević D D, Jugović D, Anićijević V J, Veselinović L, Mitrić M *et al* 2019 *Solid State Sci.* **87** 81
[26] Chen W, Lan M, Zhu D, Ji C, Feng X, Yang C *et al* 2013 *J. Mater. Chem. A* **1** 10912
[27] Kosova N V, Tsapina A M, Slobodyuk A B and Petrov S A 2015 *Electrochim. Acta* **174** 1278
[28] Zhang B, Ou X, Zheng J, Shen C, Ming L, Han Y *et al* 2014 *Electrochim. Acta* **133** 1
[29] Kim H, Shakoor R A, Park C, Lim S Y, Kim J S, Jo Y N *et al* 2013 *Adv. Funct. Mater.* **23** 1147
[30] Bard A J and Faulkner L R 2001 *Electrochemical methods: fundamentals and applications* 2nd ed (New York, United States: Wiley)
[31] Kisu K, Iwama E, Naoi W, Simon P and Naoi K 2016 *Electrochem. Commun.* **72** 10
[32] Naoi K, Kisu K, Iwama E, Nakashima S, Sakai Y, Orikasa Y *et al* 2016 *Energy Environ. Sci.* **9** 2143
[33] Gaberscek M, Moskon J, Erjavec B, Dominko R and Jamnik J 2008 *Electrochem. Solid State Lett.* **11** A170
[34] Schmidt J P, Chrobak T, Ender M, Illig J, Klotz D and Ivers-Tiffée E 2011 *J. Power Sources* **196** 5342
[35] Atebamba J-M, Moskon J, Pejovnik S and Gaberscek M 2010 *J. Electrochem. Soc.* **157** A1218
[36] Lu X, Wei H, Chiu H C, Gauvin R, Hovington P, Guerfi A *et al* 2015 *Sci. Rep.* **5** 1
[37] Shimizu D, Nishimura S, Barpanda P and Yamada A 2012 *Chem. Mater.* **24** 2598